

INVESTIGATION ON LATERAL BEHAVIOR OF CORRUGATED STEEL PLATE SHEAR WALLS WITH OPENINGS OR SLITS

En-Feng Deng ^{1,*}, Yu-Han Wang ¹, Dou-Dou Si ², Zhe Zhang ¹ and Guang-Cao Zhang ¹

¹ School of Water Conservancy and Civil Engineering, Zhengzhou University, Zhengzhou 450001, China

² School of Civil Engineering, Tongji University, Shanghai 200092, China

* (Corresponding author: E-mail: dengenfeng@zzu.edu.cn)

ABSTRACT

In place of traditional on-site construction, modular steel construction (MSC) is an excellent alternative and it is gaining popularity. The innovative construction method possesses higher construction speed and quality by moving large proportion of the building to be manufactured in the factory, which is favorable to environmental protection. Schools, hotels, and apartments have widely adopted modular steel construction as its convenience for transportation. This paper mainly focused on the lateral behavior of corrugated steel plate shear walls (CSPSWs) with openings or slits in container-like modular steel construction. A 3D finite element model (FEM) was established and validated against the test results. The failure process of the CSPSWs with opening was revealed and discussed. Further, theoretical deduction was carried out to predict the initial lateral stiffness of CSPSWs with opening and the proposed formulas agreed well with the test and simulation results. In addition, parametric analysis was performed to reveal the lateral behavior of CSPSWs with vertical slits based on the verified FEM. It indicated that the layer and location of the vertical slit have prominent influence on the initial stiffness and ultimate load of CSPSWs. Meanwhile, in order to investigate the effect of opening location on the initial stiffness of CSPSWs with openings, a parametric study was conducted and the reasonable location of the opening was recommended. The present study provides useful design guidelines for the design of CSPSWs, which is beneficial to promoting the application of modular steel construction.

ARTICLE HISTORY

Received: 12 January 2023
Revised: 12 April 2023
Accepted: 10 May 2023

KEYWORDS

Modular steel construction;
CSPSW;
Vertical slits;
Opening;
Finite element analysis;
Design consideration

Copyright © 2023 by The Hong Kong Institute of Steel Construction. All rights reserved.

1. Introduction

Modular construction, or off-site prefabricated volumetric construction, is increasingly used for hotels, schools and hospitals, which can be modularized manufactured [1][2]. A permanent modular structure is made up by the module unit prefabricated in the factory and assembled together on the construction site after transportation [3]. The main technical highlights of the innovative construction method include higher efficiency, better quality and less resource wastage. Therefore, modular construction is of particular interest across the construction industry and academia [4][5].

Lawson et al. [6], Kim and Lee [7] have conducted case studies of modular construction, indicating the superiority of modular construction. Liew et al. [8][9] proposed the prefabricated prefinished volumetric construction (PPVC) and introduced its potential practice. The lightweight concrete with different strength grades was filled in the square hollow section (SHS) to satisfy the varied load bearing requirements for columns in different layers. A review of modular building structures was presented by Lacey et al. [10]. The structural form, construction material as well as the existing inter-module connections were summarized. Among the various types of modular construction, the container-like modular steel construction has been widely employed attributable to its convenience for transportation and connecting. The nonstandard container can be transformed and finished for building function, shown as Fig. 1. The dimensions of the module units are generally in the range of 3–5m in width, 10–20m in length, and 3–4m in height. The corrugated steel plates are usually served as the surface enclosures of the module. It is necessary to decorate the corrugated steel plates with thermal insulation material to realize the building function. Meanwhile, corrugated steel plate has been proven to be an favourable lateral-force resisting component compared to steel plate shear walls (SPSWs) [11][12].

For investigating the seismic mechanism of corrugated steel plate shear walls (CSPSWs), a series of studies have been carried out. Giriunas et al. [13] found that the surface corrugated steel plates were important lateral load-resisting components for containers by numerical simulation. The strengthening effect of sidewalls cannot be ignored. Corrugated steel shear walls performed better than unstiffened steel plate shear walls (SPSWs) according to the cyclic tests conducted by Fereshteh et al. [14]. Deng et al. [15] investigated the initial stiffness of CSPSWs in modular steel construction through numerical and theoretical studies. The practical design formulas on initial stiffness of CSPSWs were derived. Yu and Chen [16] studied the stiffness strengthening effect of corrugated sidewalls in container-like modules. The initial stiffness and a simplified numerical model of CSPSWs were presented.

Finite element analysis and cyclic tests were conducted on two kinds of steel plate shear walls with non-uniform spacing slits by Lu et al [17]. It indicated that the steel plate shear wall can dissipate more energy through the development of plasticity in the strip between the slits. In addition, Lu et al. [18] conducted finite element analysis of self-centering steel plate shear walls with slits under cyclic loading, and the numerical results agreed well with the test ones. Wang et al. [19] designed an innovative modular panel with slits on steel plate shear walls, and a series of tests under cyclic load were taken to reveal its seismic characteristic. Meanwhile, considering the necessity of openings to install windows or doors for realization of building function in MSC, Ding et al. [20] conducted cyclic tests on CSPSWs with openings in modular construction. It indicated that the seismic characteristic of CSPSWs was evidently influenced owing to the opening. The initial stiffness of CSPSWs reduced rapidly as the increasing of the area of the opening. Farzampour and Laman [21] compared the mechanical behavior of CSPSWs and SPSWs with and without openings through a series of numerical studies. Given the extensive researches available on seismic performance of CSPSWs, the excellent seismic performance of CSPSWs has been verified. However, the related research on seismic behavior of CSPSWs with openings is inadequate, and few research has been focused on the lateral behavior of CSPSWs with slits.

The main focus of this paper was on the lateral performance of CSPSWs with openings or slits. Detailed finite element models (FEM) were developed firstly and verified by the previous tests conducted by the authors. In addition, the theoretical model of CSPSWs with openings was developed and the initial stiffness of CSPSWs with openings was deduced and validated. Then, the influence of the vertical slits and openings on the initial stiffness of CSPSWs was investigated through a series of parametric studies. The influence of layer of the slit, location of the slit and location of the opening was revealed. The reasonable location of the opening and design recommendation on the vertical slit were proposed, providing useful design guidelines for CSPSWs with openings or slits in modular construction.



Fig. 1 CSPSWs with openings in modular construction

2. General of the test and finite element modelling

2.1. General of the test

Four full-scale CSPSWs specimens with openings labeled as CSPSWO1–CSPSWO4 were tested by Ding et al. [20]. Table 1 shows the geometric and material characteristics of the specimens. Specimen CSPSWO1 and CSPSWO3 were designed with window opening and CSPSWO2 and CSPSWO4 were designed with door opening. The constructional columns were utilized to reinforce the edges of the opening. Fig. 2(a) shows the test device. The specimen was fixed by two hinged supports to simulate the connection between the individual modules and tested under cyclic horizontal displacement. Lateral-restraint apparatus was adopted to prevent the global twist of the specimen during the test. The seismic performance test results reported by Ding et al. [20] was used to validate the developed FEM in the following section.

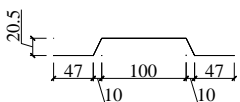
2.2. Development of the FEM

The FEM was established based on the universal software ABAQUS (Version 6.13) [22]. The established FEM is illustrated in Fig. 2(b). The FEM consists of the outer frame and the infill corrugated steel plate. The constructional columns are tied to the adjacent frame beam or frame column. The four-node shell element S4R with reduced integration is adopted to simulate the frame beam, frame column, constructional column and the infill corrugated steel plate with a mesh size of 40mm. Similarly, each infill plate is tied to the adjacent beam or column. In this way, each infill plate and the outer frame can be meshed independently using the structured meshing method. This meshing strategy is useful to avoid the irregular elements and obtain satisfactory computing efficiency. The bilinear kinematic hardening model and Von-Mise yielding criterion available in the ABAQUS metal plasticity library are employed in the FEM. The elastic modulus, yield strength, and ultimate strength are accordance with the test results, as given in Table 1. The hardening modulus equals to 0.01 times of the elastic modulus and the Poisson's ratio is set to 0.3. The bottoms of the two modular columns are pin-constrained to be consistent with the test setup. Meanwhile, the webs of the ceiling beam are restrained from out-of-plane lateral displacement, simulating the lateral restraint apparatus, as shown in Fig. 2(b).

In order to simulate the initial imperfection of the infill corrugated steel plate, linear elastic eigenvalue buckling analysis was primarily performed using the subspace iteration method available in ABAQUS to extract the buckling modes. Global buckling occurred in the first buckling mode for all the four specimens, as shown in Fig.3. The geometric imperfection amplitude was set to be $H/200$ of the first buckling mode, where H was the height of specimen [23][24]. Then, the cyclic displacement load the same as the test was applied at one end of the ceiling beam to simulate the cyclic load. The ABAQUS/implicit module was used to solve the response of the FEM.

Table 1

The geometric and material properties of the CSPSW specimens with openings

Specimen	t (mm)	Opening		Section of the specimen (mm)	E (GPa)	f_y (MPa)	f_u (MPa)
		Size $l \times h$ (mm)	Function				
CSPSWO1	1.70	1000×1600	Window		195	388	511
CSPSWO2	1.58	1000×2290	Door				
CSPSWO3	1.68	1800×1600	Window	□150×100×6	195	394	504
CSPSWO4	1.70	1800×2290	Door	frame beam/ frame column			

Note: t : measured thickness of the corrugated steel plate; l : length of the opening; h : height of the opening; E : elastic modulus; f_y : yield strength; f_u : ultimate tensile strength.

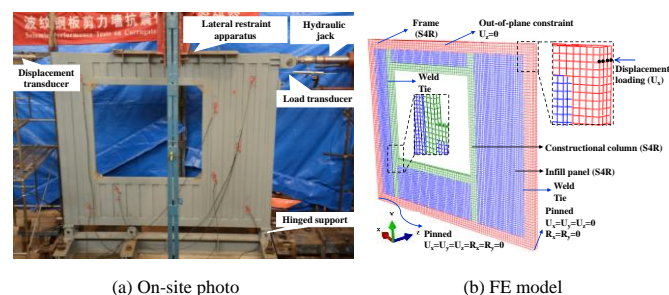


Fig. 2 Test setup and FEM for CSPSWs with openings

2.3. Validation and discussion

A comparison of the hysteretic curve and the skeleton curve between the test results and finite element analysis (FEA) is shown in Fig. 4. Generally, the FEA agrees well with the test results. In addition, the comparisons between the initial stiffness (K_0) and ultimate load (F_u) of the specimens are listed in Table 2. The positive loading is signed as “+”, while the negative loading is signed as “-”. As shown in Fig. 2(a), the push (from right to left) applied on the specimen is defined as positive loading and the pull (from left to right) is defined as negative loading.

All the specimens failed in three stages: the elastic stage, the yield stage, and the failure stage. The FEA almost coincides with the test results in the elastic stage. The comparisons in Table 2 indicate that the FEM overestimated the initial stiffness (K_0) of the specimens averagely with FEA-to-test ratios ranging from 1.01 to 1.25 with a mean value of 1.16 and coefficient of variation (COV) of 0.07. The overestimation may be caused by the difference of boundary conditions between the test setup and FEM. The out-of-plane displacement of the web of the ceiling beam is restrained ideally in the FEM. However, a gap with a width of 10mm is necessary between the lateral restraint apparatus and the specimen for the convenience of installation, as shown in Fig. 2(a). The gap may result in slight global twist of the specimen in the positive loading, leading to the lower K_0 of the test results, especially in the positive direction. The FEM also simulates well of the test results in the yield development stage. The FEA-to-test ratio of the ultimate load (F_u) ranges from 0.99 to 1.09 with a mean value of 1.02 and COV of 0.05. In the failure stage, the fracture of the infill panel and the constructional column develops and aggravates rapidly as the accumulation of damage. The damage is particularly concentrated in the corner regions of the opening, as shown in Fig. 5. The fracture of the constructional column and infill panel results in the decline of the load-bearing capacity in the failure stage. However, the fracture is not considered in the FEM, leading to the higher load of FEA than the test results, as shown in Fig. 4.

The comparisons of failure mode between test results and FEA are shown in Fig. 5. It indicates that the FEM predicts well the failure mode of the specimens, including the global buckling of the infill panel and the local buckling of the constructional columns in the corners of the opening.

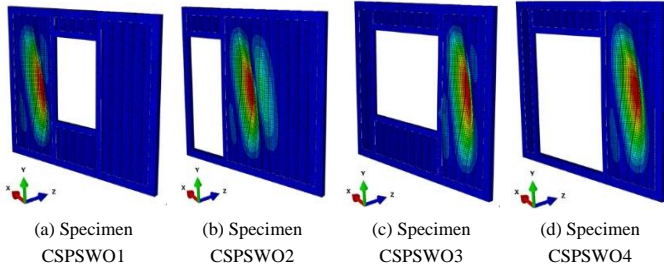


Fig. 3 First buckling mode of CSPSWs with openings

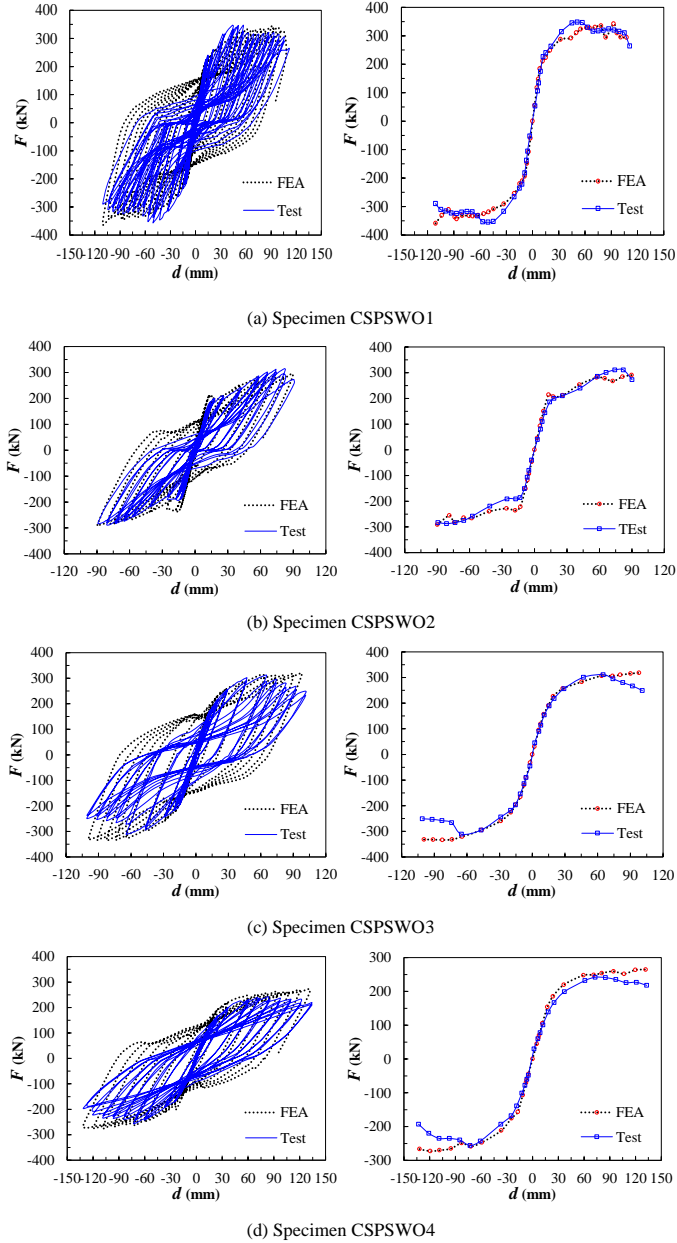


Fig. 4 Comparisons of hysteretic and skeleton curves between test and FEA

The above comparisons and discussion verify the reliability of the FEM, which can be used for further analysis. The failure process of the four specimens is shown in Fig. 6. It is found that the damage mainly exists in the corner regions of the openings due to stress concentration, as the increasing of the inter-story drift ratio. Local buckling and fracture occur in the constructional column in the corner regions, indicating the consistence of FEA and test results. The failure inter-story drifts of CSPSWO1~CSPSWO4 are 0.0389rad, 0.0315rad, 0.0354rad and 0.0467rad, respectively. Specimen CSPSWO2 performs the worst deformation capacity. The door opening locates in the corner of the outer frame, as shown in Fig. 5(b). The stress concentration in the corners of the opening leads to the undesired fracture of the weld between the frame beam and the frame column. The specimen loses load-bearing capacity due to the fracture and performs the worst deformation capacity and ductility. As a result, the opening should be located off the diagonal tension field of the infill panel.

Table 2

Validation of the FEM by comparisons of characteristic values between test and FEA

Specimen	Loading direction	K_0 (kN/mm)			F_u (kN)		
		Test	FEA	FEA/Test	Test	FEA	FEA/Test
CSPSWO1	+	20.4	25.4	1.25	347	342	0.99
	—	21.2	25.4	1.20	356	360	1.01
CSPSWO2	+	13.3	16.3	1.23	315	291	0.92
	—	16.1	16.3	1.01	291	291	1.00
CSPSWO3	+	12.6	14.7	1.17	313	318	1.02
	—	12.3	14.7	1.20	312	333	1.07
CSPSWO4	+	6.80	7.80	1.15	242	265	1.09
	—	7.10	7.80	1.10	256	273	1.07
Mean	-	-	-	1.16	-	-	1.02
COV	-	-	-	0.07	-	-	0.05

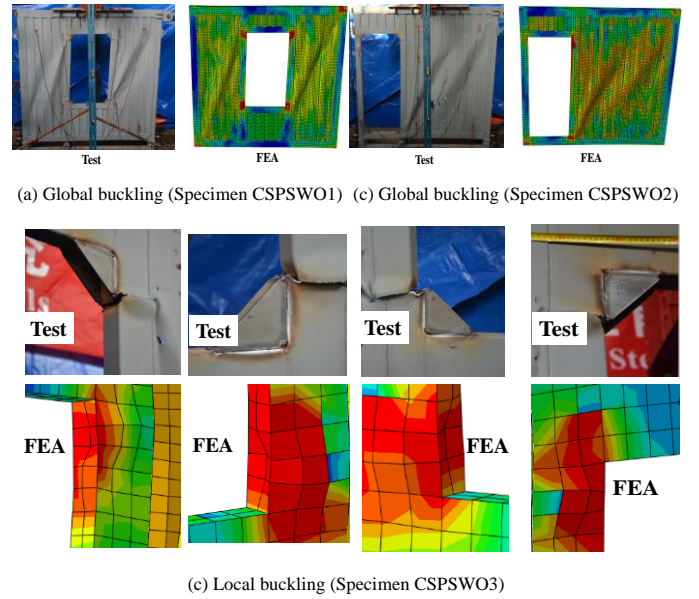


Fig. 5 Comparisons of failure mode between test and FEA

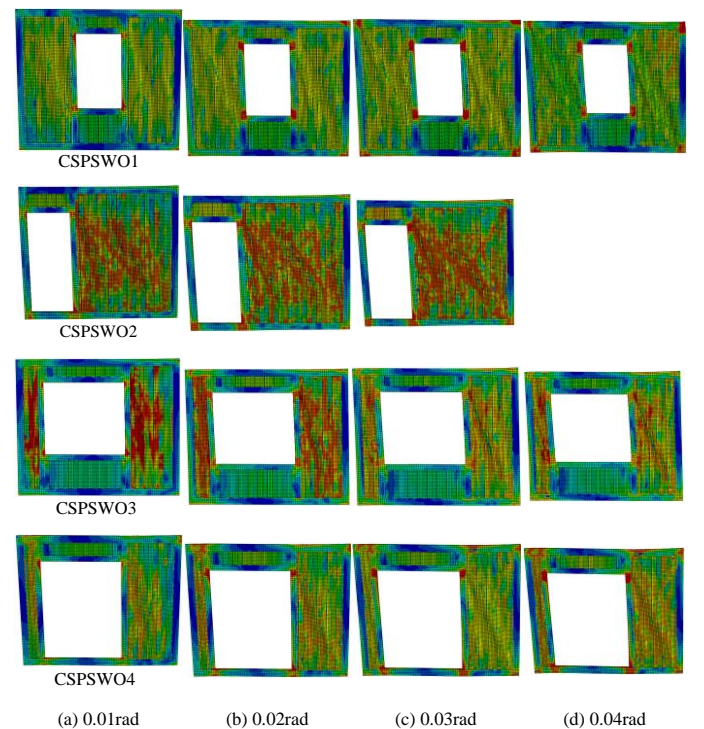


Fig. 6 Failure process of the CSPSW specimens with openings

3. Theoretical modelling of CSPSWs with openings

3.1. General

The initial stiffness of the infill panel (K_w) was derived by Deng et al. [15] as following:

$$K_w = \frac{\gamma}{\frac{H_e^3}{12E \cdot I_z} + \frac{3.12 \cdot H_e}{E \cdot \eta \cdot L_e \cdot t}} \quad (1)$$

where, the thickness and the elastic modulus of the infill panel are denoted by t and E , respectively; the effective length and height of the panel are described by L_e and H_e , respectively; η indicates the shape factor of the section; as a result of elastic buckling and geometrical imperfections, the initial stiffness is reduced and it is described by γ , based on the following equation.

$$\gamma = 0.014 \ln(L_e / H_e) - 0.118 \ln(\lambda) + 1.24 \quad (2)$$

where, λ represents the relative height-to-thickness ratio of the infill panel, which can be expressed as Eq. (3). f_y denotes the yield strength of the infill panel.

$$\lambda = \frac{H_e}{t \cdot \sqrt{\frac{235}{f_y}}} \quad (3)$$

Shape factor is a measure of the ratio between the unfolding length and the net length of the corrugated steel plate and it is denoted by η .

$$\eta = \frac{a+d+c}{a+b+c} \quad (4)$$

where, a , b , c and d denote the geometrical parameters, as shown in Fig. 7.

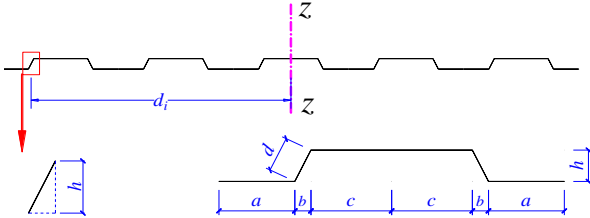


Fig. 7 Cross section characteristics of the corrugated steel plate

The mechanical model of CSPSWs with openings under horizontal force f was shown in Fig.8. The infill panel was divided into several regions along the edges of the opening. Each region was equivalent to a spring with elastic stiffness equals to the corresponding corrugated steel plate. The initial stiffness of the spring K_{ij} can be determined by Eq. (1), where K_{ij} denotes initial stiffness of the i th row j th column region. Taking the window opening in Fig. 8(a) for example, the following equation can be obtained according to the compatibility of deformation.

$$\frac{f}{K_{00}} = \frac{f}{K_1} + \frac{\alpha_{21} \cdot f}{K_{21}} + \frac{f}{K_3} \quad (5)$$

$$\frac{f}{K_{00}} = \frac{f}{K_1} + \frac{\alpha_{22} \cdot f}{K_{22}} + \frac{f}{K_3} \quad (6)$$

where, K_{00} denotes the initial stiffness of the infill panel with opening; α_{21} and α_{22} denote the distribution coefficient of horizontal force in the 2nd layer; K_1 and K_3 denote the initial stiffness of the 1st and 3rd layers, which can be determined by the following equations.

$$K_1 = K_{11} + K_{12} + K_{13} \quad (7)$$

$$K_3 = K_{31} + K_{32} + K_{33} \quad (8)$$

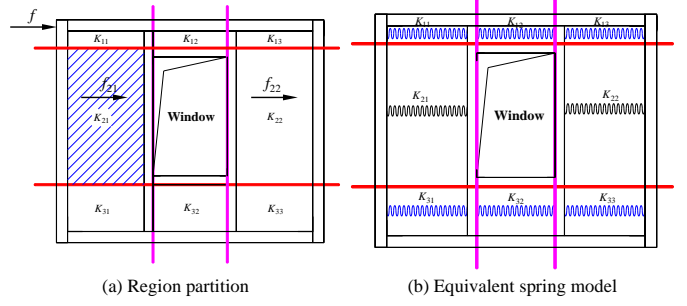


Fig. 8 Mechanical model of CSPSWs with openings

The horizontal force in the 2nd layer was distributed proportionally to the stiffness of the region, yielding the following equations.

$$\alpha_{21} + \alpha_{22} = 1 \quad (9)$$

$$\frac{\alpha_{21}}{K_{21}} = \frac{\alpha_{22}}{K_{22}} \quad (10)$$

Substituting Eqs. (7) ~ (10) into Eq. (5) yields the initial stiffness of the infill panel with openings, as expressed in Eq. (11).

$$K_{00} = \frac{1}{\frac{1}{K_{11} + K_{11} + K_{11}} + \frac{1}{K_{21} + K_{22}} + \frac{1}{K_{31} + K_{32} + K_{33}}} \quad (11)$$

Similarly, Eq. (11) can be generalized as Eq. (12) to calculate the initial stiffness of the infill panel with arbitrary openings.

$$K_{00} = \frac{1}{\sum_{j=1}^n \frac{1}{\sum_{i=1}^m K_{ij}}} \quad (12)$$

where, m and n denote the column number and row number of the region after partition.

Considering the contribution of the outer frame to the initial stiffness of CSPSWs with openings, the following equation can be given to predict the initial stiffness of the CSPSWs with openings (K_0).

$$K_0 = \frac{1}{\frac{H^3}{6E_1 I_1} (3\phi^2 - 3\phi + 1) + \frac{LH^2 \phi^2}{12E_2 I_2} + \frac{(1-\phi)^2 H^2 L}{12E_3 I_3}} + \frac{1}{\sum_{j=1}^n \frac{1}{\sum_{i=1}^m K_{ij}}} \quad (13)$$

3.2. Verification of the theoretical modelling

In this section, the accuracy of the theoretical derivation was validated by comparing the theoretical values with the test and numerical results. The tests conducted by Ding et al. [15] were adopted and the developed FEM in Section 2 was used to provide more validating datas. Fig 9 and Table 3 provide comparisons between theoretical values (K_0) and the related test and numerical results. The specimens used for finite element analysis (FEA) were labeled by the specimen number and the thickness of the infill panel. For example, specimen CSPSWO1-0.8 means the thickness of the infill corrugated steel plate is 0.8mm and the other geometric dimensions are the same as Specimen CSPSWO1.

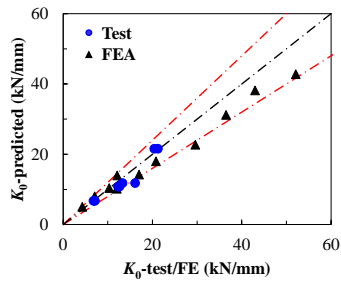
The comparisons indicated that Eq. (13) was effective to predict the initial stiffness of CSPSW with openings. In terms of K_0 -to-test and K_0 -to-FE ratios, the mean value was 0.93 and the coefficient of variation was 0.13. As discussed in Section 2.2, the space between the lateral restraint apparatus and specimens

in the test led to the lower stiffness in the positive direction than the negative direction. Therefore, the K_0 -to-test ratio was averagely higher in the positive direction than that of the negative direction. These validations verify that Eq. (13) derived in this paper is reasonable to predict the initial stiffness of CSPSWs with openings, which will be analysed in depth in the following section.

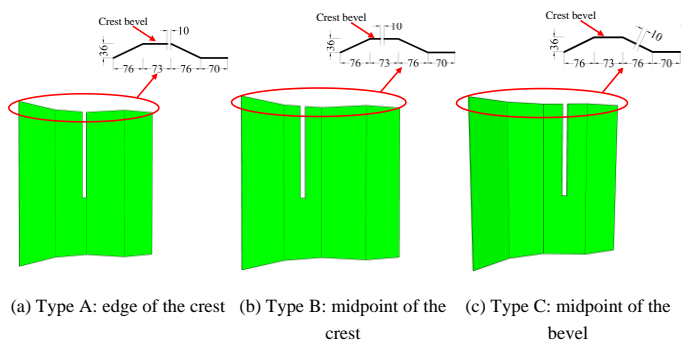
Table 3

Validation of the theoretical formulas against the test results and FEA

Specimen		$L \times H$ (m×m)	$l \times h$ (m×m)	Test (kN/mm)	K_0 (kN/mm)	K_0/Test
CSPSWO1	+	3.6×3.0	1.00×1.60	20.4	21.6	1.06
	−	3.6×3.0	1.00×1.60	21.2	21.6	1.02
CSPSWO2	+	3.6×3.0	1.00×2.29	13.3	11.8	0.89
	−	3.6×3.0	1.00×2.29	16.1	11.8	0.73
CSPSWO3	+	3.6×3.0	1.80×1.60	12.6	10.8	0.86
	−	3.6×3.0	1.80×1.60	12.3	10.8	0.88
CSPSWO4	+	3.6×3.0	1.80×2.29	6.80	6.76	0.99
	−	3.6×3.0	1.80×2.29	7.10	6.76	0.95
Specimen		$L \times H$ (m×m)	$l \times h$ (m×m)	FEA (kN/mm)	K_0 (kN/mm)	K_0/FEA
CSPSWO1-0.8		3.6×3.0	1.00×1.60	12.1	14.0	1.15
CSPSWO1-2.4		3.6×3.0	1.00×1.60	36.5	31.2	0.85
CSPSWO1-3.2		3.6×3.0	1.00×1.60	52.1	42.8	0.82
CSPSWO2-0.8		3.6×3.0	1.00×2.29	10.3	10.4	1.00
CSPSWO2-2.4		3.6×3.0	1.00×2.29	43.0	38.2	0.89
CSPSWO2-3.2		3.6×3.0	1.00×2.29	61.8	51.1	0.83
CSPSWO3-0.8		3.6×3.0	1.80×1.60	7.08	8.03	1.13
CSPSWO3-2.4		3.6×3.0	1.80×1.60	20.8	18.0	0.87
CSPSWO3-3.2		3.6×3.0	1.80×1.60	29.6	22.7	0.77
CSPSWO4-0.8		3.6×3.0	1.80×2.29	4.27	5.05	1.18
CSPSWO4-2.4		3.6×3.0	1.80×2.29	12.0	10.2	0.85
CSPSWO4-3.2		3.6×3.0	1.80×2.29	17.0	14.2	0.84
Mean		-	-	-	-	0.93
COV		-	-	-	-	0.13

**Fig. 9** Validation of the theoretical formulas

4. Parametric analysis on CSPSWs with vertical slits

**Fig. 10** Different locations of the vertical slits

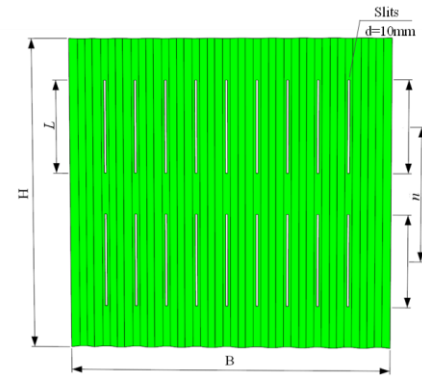
In this section, the verified FEM was used to analyse the factors influencing the lateral behaviour of CSPSWs with vertical slits. The considered parameters include thickness of the infill panel, the location and layer of the slits. The detailed dimensions of the models in parametric study and FEA results were listed in Table 4. It should be mentioned that the spacing of each slit is 295mm and the width of the slit was 10mm. The different locations of the vertical slits are shown in Fig. 10. Fig. 11 shows CSPSWs models with different layers of vertical slits.

Table 4

Parameters and analysis results of CSPSWs with slits

Specimen	Slit	n	Location of the vertical slits	t (mm)	L (mm)	P_u (kN)	K_0 (kN/mm)
SW-1	Yes	1	B	2.0	3000	85.41	11.16
SW-2	Yes	1	C	2.0	3000	66.96	6.83
SW-3	Yes	1	B	3.0	3000	144.97	16.60
SW-4	Yes	1	C	3.0	3000	177.35	9.54
SW-5	Yes	1	B	4.0	3000	247.82	21.55
SW-6	Yes	1	C	4.0	3000	221.44	12.87
SW-7	Yes	1	B	5.0	3000	337.24	26.32
SW-8	Yes	1	C	5.0	3000	273.40	15.57
SW-9	Yes	1	B	6.0	3000	418.06	30.82
SW-10	Yes	1	C	6.0	3000	321.42	18.38
SW-11	Yes	1	B	8.0	3000	509.34	38.74
SW-12	Yes	1	B	8.0	3000	429.34	23.75
SW-13	Yes	1	B	6.0	3000	504.59	36.87
SW-14	Yes	2	B	6.0	1500	842.27	71.80
SW-15	Yes	3	B	6.0	1000	1036.78	92.38
SW-16	Yes	1	A	6.0	3000	466.90	34.20
SW-17	Yes	2	A	6.0	1500	760.60	68.58
SW-18	Yes	3	A	6.0	1000	934.47	90.44
SW-19	Yes	1	C	6.0	3000	467.38	23.78
SW-20	Yes	2	C	6.0	1500	740.63	47.83
SW-21	Yes	3	C	6.0	1000	910.62	69.58
SW-22	No	—	—	4.0	—	486.41	76.01
SW-23	No	—	—	6.0	—	576.70	89.59

Note: n : number of the layers of the slits; t : thickness of the corrugated steel plate; L : length of the slits.

**Fig. 11** Details of CSPSWs

4.1. Influence of the vertical slit

Fig. 12 and Fig. 13 showed the first buckling mode of the CSPSWs with and without slits with two different thickness of the corrugated steel plate. It can be found out that global buckling occurred for the specimens without slit, i.e., Specimen SW-22 and Specimen SW-23. However, local buckling occurred for

the wall limbs between the slits for the specimens with slits. This finding suggested that the vertical slits changed the load bearing mechanism of CSPSWs. Local buckling occurred for the specimen with slits, which was favorable to dissipate energy under earthquake.

The load-displacement curves of Specimen SW-5, SW-6 and SW-22 were displayed by Fig. 14. As shown in Fig.14, before the lateral displacement reaches 9.8mm, Specimen SW-22 which is without slits behaves almost in an elastic manner and global buckling can be observed. With the temporary occurrence of the “negative stiffness”, the decrease of load-displacement curve can be observed correspondingly. With the increasing of displacement, tension strip develops after drifts of 10.3mm and the load bearing capacity begins to increase. Different from Specimen SW-22, shear yielding occurred for Specimen SW-5 and SW-6 which were with slits. Each specimen failed due to tension field development, fracture propagation, local buckling and fracture of the infill panel. The elastic stage, the yielding development stage and the failure stage occurred in sequence during the damage process. The results indicate that the initial stiffness and ultimate load of the CSPSWs were significantly reduced due to the slits. Specifically, the initial stiffness and ultimate load of Specimen SW-22 is 96.3% and 252.7% higher than Specimen SW-5 and those of Specimen SW-6 is 119.7% and 490.6% lower than Specimen SW-22. However, the ductility of CSPSWs with slits was improved due to the fact that the failure mode of CSPSWs changed from global buckling to shear yielding.

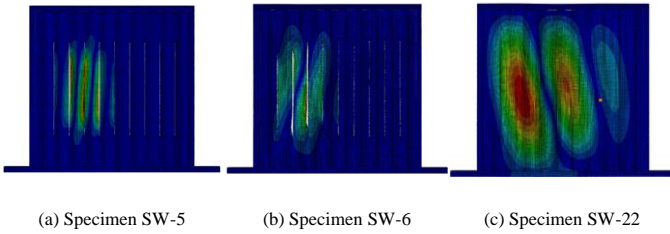


Fig. 12 First buckling mode of CSPSWs with and without slits ($t=4.0\text{mm}$)

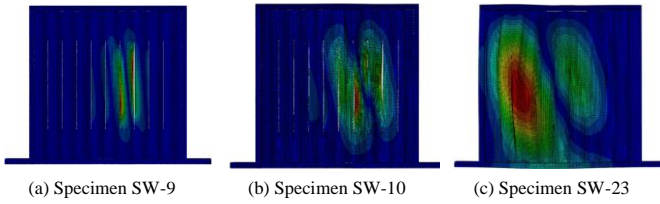


Fig. 13 First buckling mode model of CSPSWs with and without slits ($t=6.0\text{mm}$)

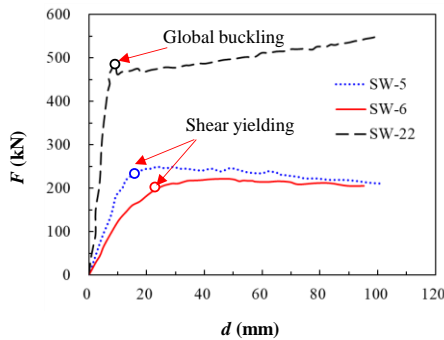


Fig. 14 Influence of vertical slits on lateral load-displacement curve of CSPSWs

4.2. Influence of layers of the vertical slit

Fig. 15 shows the first buckling model of Specimens SW-13 to SW-21. Local buckling can be found for the Specimens with one layer of vertical slit. With the increasing of layers of the vertical slit, the first buckling model of the specimen was close to global buckling, resulting in larger plastic area of the infill panel. This finding suggested that increasing layers of the vertical slit may increase the energy dissipation capacity of CSPSWs. Meanwhile, the buckling mode of the specimens with three layers of vertical slits was similar to the CSPSWs without slits. Therefore, it can be concluded that increasing the layers of the slit can improve the integrity and mechanical property of CSPSWs.

Fig. 16 shows the load-displacement curves of Specimen SW-13 to SW-21. As shown in the picture, both of the initial stiffness and ultimate load of the specimen improved with the increasing of the layers of the vertical slit. The initial stiffness of specimens with three layer slits SW-18 and SW-15 are 100.1% and 105.5% higher than specimens with one layer slits SW-16 and SW-13. Moreover, the initial stiffness of specimen SW-16 and SW-13 are 164.4% and 150.6% lower than those of Specimens SW-18 and SW-15. Comparing with Specimen SW-19, the initial stiffness and ultimate load of Specimen SW-21 increase by 192.6% and 94.7%, respectively. It indicated that the lateral behavior of CSPSWs was obviously affected by the layer of the slit. It is suggested to increase the layer of slit to improve the lateral behavior of CSPSWs with slits.

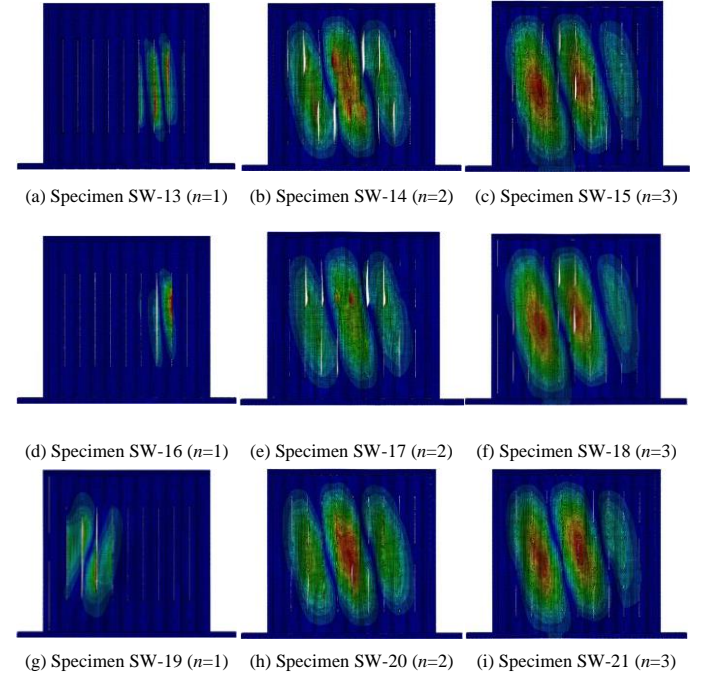


Fig. 15 First buckling model of Specimens with different layers of the vertical slit

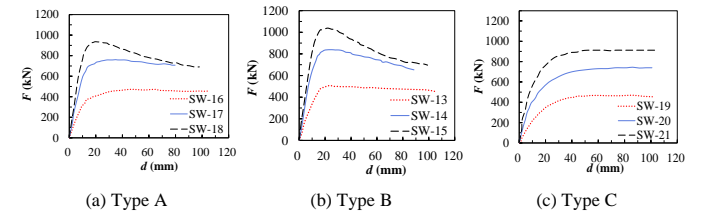


Fig. 16 Influence of layers of vertical slits on lateral load-displacement curve of CSPSWs

4.3. Influence of location of the vertical slits

Fig. 17 showed the load-displacement curves of specimens with different location of the slit. It can be seen that Specimens SW-13, SW-14, SW-15 performed better than other specimens with the same layer of vertical slit. With the increasing of the displacement, the curves of Specimen SW-13 to SW-15 whose slits are on the crest occur the descent stage. Meanwhile, the curves of Specimen SW-19 to SW-21 occur ascending stage and tend to be stable. It can be concluded from Table 4 that it is better to set the slit at the midpoint of the crest to obtain higher initial stiffness and load bearing capacity. Furthermore, the difference can be more obvious with the increasing of the layer of the slits.

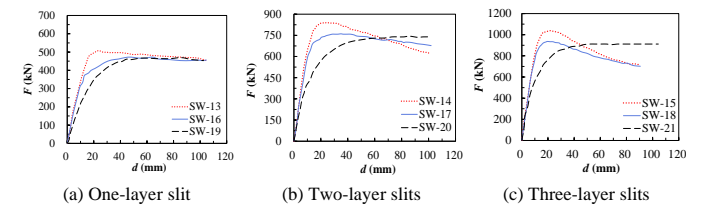


Fig. 17 Load-displacement curve of Specimens with different location of slits

5. Parametric analysis on CSPSWs with openings

Conventionally, the vertical position of the opening is determined by the building function. The bottom edge of the window is set to a fixed value and the bottom edge of the door is required to fall on the ground. Therefore, only the horizontal position of the opening was considered and discussed. The axes of the opening are displayed in Fig. 18. Each specimen is divided into seven parts along the horizontal direction averagely. Specimens CSPSWO1~CSPSWO4 were used for analysis. Each specimen with different thickness (t) and different height of the crest of the corrugated steel plate (h) was analyzed and discussed to provide a better understanding on how the location of the opening affects the specimens and to explore the proper design recommendation. The influence of the location of the opening on initial stiffness of CSPSWs with openings is shown in Fig. 19.

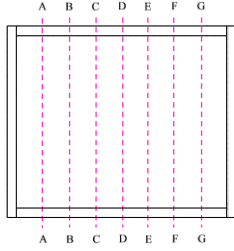


Fig. 18 The axes of the opening for parametric analysis

It is indicated that the location of the opening influence the initial stiffness of CSPSW significantly, as shown in Fig. 19. The specimens have the least initial stiffness when the opening is located in the middle of the specimen, i.e., the axis of the opening is D. On the contrary, the specimens have the largest initial stiffness when the opening is located in the edges of the specimen, i.e., the axis of the opening is A or G. It can be concluded that it is the most unfavorable to locate the opening in the middle of the specimen. The influence of the location of the opening is especially obvious with higher t and h . Take Specimen CSPSWO1 as an example, the initial stiffness of the specimen is 119.5kN/mm and 68.5kN/mm when the axis of the opening is A and D, respectively, with the thickness of the infill panel is fixed to 4mm. The initial stiffness of the specimen is 1.74 times higher with the opening in the edge than in the middle. The initial stiffness of the specimen is 56.2kN/mm and 31.9kN/mm when the axis of the opening is A and D, respectively, with the height of the crest of the corrugated steel plate is fixed to 80mm. The initial stiffness of the specimen is 1.76 times higher with the opening in the edge than in the middle. Therefore, it is recommended to locate the opening close to the edges of the specimen to alleviate the weakening of the opening on the initial stiffness of CSPSWs. As discussed in Section 2.2, it is recommended that the opening should not be placed at the end of the diagonal tension field to ensure the deformation capacity and ductility of the specimen. Therefore, the location of the opening is recommended as shown in Fig. 20.

6. Conclusions

This paper investigated the lateral behavior of CSPSWs with openings or slits in modular steel construction numerically and theoretically. A finite element model was developed and the numerical results are consistent to the test results, which verifies the reliability of the FEM. The failure process of the specimens was revealed and evaluated. In addition, CSPSWs were studied parametrically for initial stiffness and ultimate load considering parameters related to the vertical slit and the opening. The influence of the vertical slit or openings on lateral behavior of CSPSWs was revealed and discussed in detail. The design consideration of the openings and slits was recommended based on the present study. Following are the main conclusions.

- (1) CSPSWs with openings is simulated using the developed FEM, including the initial stiffness, ultimate shear capacity, and failure mode.
- (2) Stress concentration exists in the corner regions of the opening. It is recommended that the opening should be located off the end of the diagonal tension field to guarantee the deformation capacity and ductility of the specimen.
- (3) Compared with the CSPSWs without slits, the ultimate load and initial stiffness of CSPSWs with slits are reduced significantly. Meanwhile, the failure mode of the CSPSWs with slits changed from global buckling to shear yielding.
- (4) The initial stiffness and ultimate load of CSPSWs improved with the increasing of the layer of slits. It is better to set the slit at the midpoint of the crest to obtain higher initial stiffness and load bearing capacity.
- (5) The location of the opening impacts the initial stiffness of CSPSWs obviously. The opening is suggested to be located at the edge of the specimen to obtain higher initial stiffness.

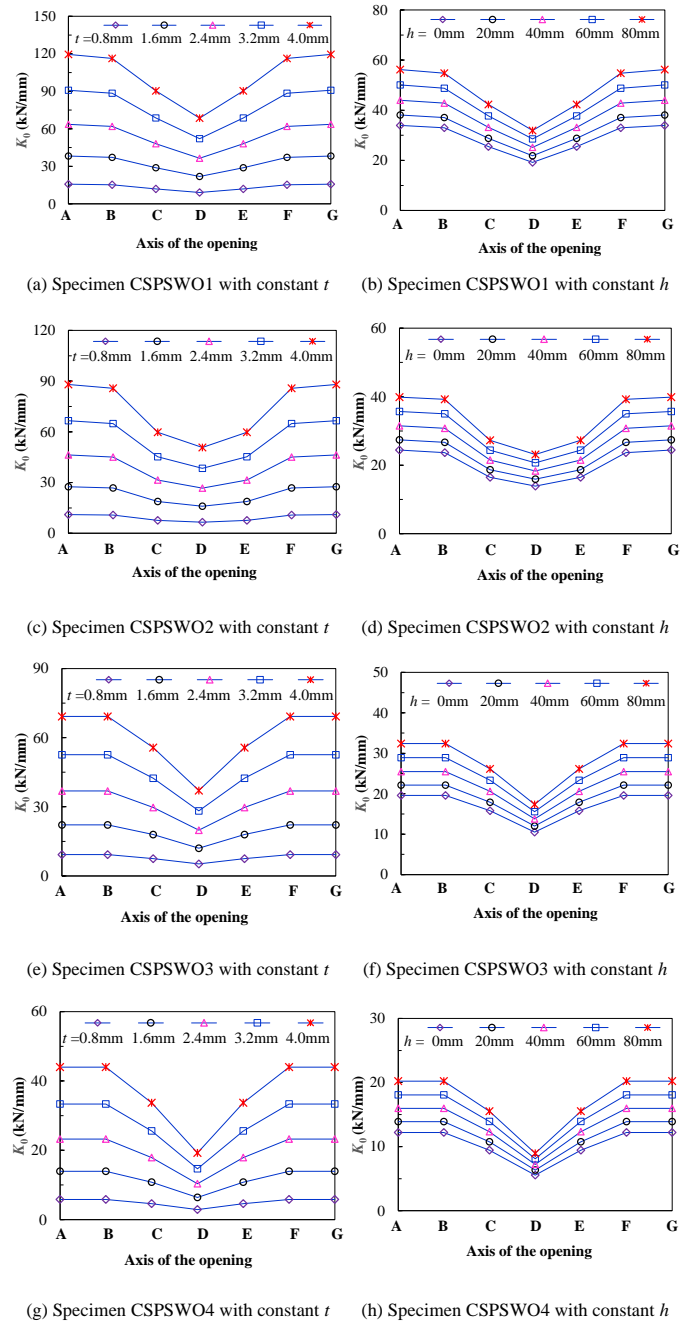


Fig. 19 Influence of the location of the opening on initial stiffness of CSPSWs

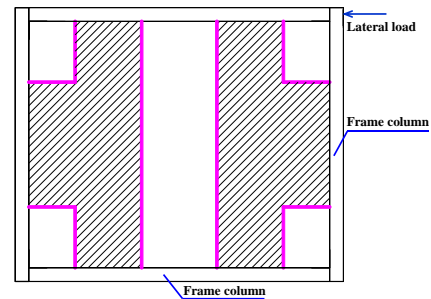


Fig. 20 Suggested location for opening (hatched)

Acknowledgements

The reported research work was sponsored by the National Natural Science Foundation of China (Grant Nos. 52378206 and 51908511), Young Talent Lifting Project of Henan Province (No. 2023HYTP015) and the Program for Innovative Research Team (in Science and Technology) in University of Henan Province (Grant No. 23IRTSTHN006).

References

- [1] Li, G.Q., Cao K., Lu, Y. EFFECTIVE LENGTH FACTOR OF COLUMNS IN NON-SWAY MODULAR STEEL BUILDINGS, *Adv. Steel Con*, 2017, 13(4): 412-426.
- [2] Liu, H.B., Zhou, Y. and Chen, Z.U. STRUCTURAL PERFORMANCE AND DESIGN METHOD OF NEW MORTISE-TENON FULL STEEL-TUBE SCAFFOLD, *Adv. Steel Con*, 2018, 14(2), 291-307.
- [3] Park K.S., Moon J., Lee S.S., Bae K.W. and Charles W.R. Embedded steel column-to-foundation connection for a modular structural system. *Eng Struct*, 2016, 110: 244-257.
- [4] Sanches R, Mercan O, Roberts B. Experimental investigations of vertical posttensioned connection for modular steel structures. *Eng Struct*, 2018, 175: 776-789.
- [5] Deng E.F., Zong L., Ding Y., Zhang Z., Zhang J.F., Shi F.W., Cai L.M., Gao S.C. Seismic performance of mid-to-high rise modular steel construction - A critical review. *Thin Wall Struct*, 2020, 155: 106924.
- [6] Lawson RM, Ray O and Chris G. *Design in Modular Construction*. CRC Press, Boca Raton, FL, 2014.
- [7] Kim J.Y., Lee J.K. A basic study on the application of modular construction, *J Korean Hou Asso*, 2014, 25(4): 39-46.
- [8] Liew J.Y.R., Dai Z. and Chua Y.S. Steel concrete composite systems for modular construction of high-rise buildings. *Proceedings of the 12th International Conference on Advances in Steel-Concrete Composite Structures*, 2018, València, Spain, June.
- [9] Liew J.Y.R., Dai Z. and Wang Y. Prefabricated prefinished volumetric construction in high-rise buildings. *Proceedings of the 11th Pacific Structural Steel Conference*, 2016, Shanghai, China, October.
- [10] Lacey A.W., Chen W.S., Hao H., Bi K.M. Structural response of modular buildings—an overview. *J Build Eng*, 2018, 16: 45-56.
- [11] Cao, Q., Huang, J.Y. Experimental study and numerical simulation of corrugated steel plate shear walls subjected to cyclic loads. *Thin Wall Struct*, 2018, 123: 306-317.
- [12] Qiu, J., Zhao, Q.H., Wang, ZY. Lateral behavior of trapezoidally corrugated wall plates in steel plate shear walls, Part 1: Elastic buckling. *Thin Wall Struct*, 2022, 174: 109104.
- [13] Giriunas K., Sezen H. and Dupaux R.B. Evaluation, modelling, and analysis of shipping container building structures. *Eng Struct*, 2012, 43: 48-57.
- [14] Fereshteh E, Massood M, Abolhassan V. Experimental study on cyclic behavior of trapezoidally corrugated steel shear walls. *Eng Struct*, 2013, 48: 750-762.
- [15] Deng E.F., Zong L., Ding Y. Numerical and analytical study on initial stiffness of corrugated steel plate shear walls in modular construction. *Steel Compos Struct*, 2019, 32(3): 347-359.
- [16] Yu Y.J., Chen Z.H. Rigidity of corrugated plate sidewalls and its effect on the modular structural design. *Eng Struct*, 2018, 175: 191-200.
- [17] Lu, J.Y., Qiao, X.D., Liao, J.. Experimental study and numerical simulation on steel plate shear walls with non-uniform spacing slits. *Interna J Steel Struct*, 2016, 16(4): 1373-1380.
- [18] Lu, J.Y., Zhang H.Y., Yu S. Study on seismic behaviors of self-centering steel plate shear walls with slits. *J Constr Steel Res*, 2021, 185: 106878.
- [19] Wang W., Kong J.H., Zhang Y.F. Seismic Behavior of Self-Centering Modular Panel with Slit Steel Plate Shear Walls: Experimental Testing. *J Struct Eng*, 2018, 144(1): 04017179.
- [20] Ding Y., Deng E.F., Zong L., Dai X.M., Lou N., Chen Y. Cyclic tests on corrugated steel plate shear walls with openings in modularized-construction. *J Constr Steel Res*, 2017, 138: 675-691.
- [21] Farzampour A., Laman J.A. Behavior prediction of corrugated steel plate shear walls with openings, *J Constr Steel Res*, 2015, 114: 258-268.
- [22] ABAQUS (2013), User manual Version 6.13. DS SIMULIA Corp, Providence, RI, USA.
- [23] Bahrebar M., Kabir M.Z., Zirakian T., Hajsadeghi M., Lim J.P.B. Structural performance assessment of trapezoidally-corrugated and centrally-perforated plate shear walls, 2016, *J Constr Steel Res*, 122: 584-594.
- [24] Eurocode (2003), *Design of Steel Structures. Part 1.5: Plated Structural elements*, European Committee for Standardization; Brussels, Belgium.